

Non-contact mechanics of soft and liquid interfaces by hydrodynamic confinement using a frequency-modulated AFM

L. Corral, C. Curtil, M. Lagaize, M. Leonetti, and H.R. Klein*

Aix-Marseille Univ, CINaM, Marseille, France

E-mail: hubert.klein@univ-amu.fr

Abstract

Measuring the mechanical response of liquid interfaces without direct contact remains a major experimental challenge, particularly in liquid–liquid systems where no solid reference exists. Here, we develop a frequency-modulation atomic force microscopy (FM-AFM) method that probes liquid interfaces through hydrodynamic confinement of a viscous liquid film between an oscillating probe and the interface. This approach provides simultaneous access to the elastic and dissipative components of the interfacial mechanical impedance. The method is first quantitatively validated on a liquid–solid interface, where the measured impedance and confinement thickness agree with elastohydrodynamic theory over nearly one decade in elastic modulus. It is then applied to a liquid–liquid interface which exhibits a purely viscous response. As a result of the absence of elastic restoring force, the confinement thickness increases to micrometric values. These original measurements demonstrate that hydrodynamic confinement provides a quantitative, non-contact probe of liquid interfaces and opens new perspectives for investigating complex and highly deformable systems such as polymer films, membranes, and capsules.

Introduction

Liquid interfaces play a central role in a wide range of physical, chemical, and biological processes, including wetting, emulsion stability, droplet deformation, and thin-film dynamics.¹ At these interfaces, the mechanical response results from the interplay between viscous flow within the liquid phases and elastic or capillary deformation of the interface.² Characterizing this response at small length scales is therefore essential for understanding interactions between fluids and soft matter at micro- and nanometric scales.

Measuring the mechanical properties of soft interfaces is challenging, particularly in the case of liquid-liquid systems. In contrast to solid substrates, a liquid interface cannot sustain a direct mechanical contact: any solid probe brought into contact with the interface inevitably penetrates it. As a result, accessing the intrinsic interfacial mechanical response requires contactless approaches. Here, the interaction between the probe and the interface is mediated by a confined liquid film. In this configuration, the measured response results from a hydrodynamic stress generated by the oscillatory flow induced by the probe's movement, and not from a direct mechanical contact.

Over the past decades, interfacial mechanical properties have mainly been investigated using macroscopic or mesoscopic techniques. The Langmuir trough allows the study of monolayers under controlled lateral compression,³ while the Wilhelmy plate method provides access to surface tension through force measurements on a partially immersed plate.⁴ Dynamic methods such as oscillating or spinning drop techniques probe interfacial tension and viscosity.^{5,6} Other approaches, including micropipette aspiration⁷ or quartz crystal micro balance with dissipation (QCM-D),⁸ give access to interfacial viscoelasticity. However, they generally do not allow a clear separation between elastic and dissipative contributions, nor do they operate under strictly contactless conditions.

At smaller length scales, hydrodynamic models based on lubrication theory have been developed to describe the drainage of thin liquid films, and to relate measured forces to viscous dissipation and elastic deformation.⁹⁻¹¹ In particular, E. Charlaix group proposed a

complete elastohydrodynamic (EHD) description of oscillatory drainage in a thin liquid film confined between a rigid probe and a soft elastic substrate.¹² In this framework, the real and imaginary parts of the mechanical impedance directly reflect elastic deformation and viscous dissipation, providing a quantitative route to separate conservative and dissipative contributions in viscoelastic systems. Frequency-modulated atomic force microscopy (FM-AFM) has also been successfully used to measure hydrodynamic forces in liquids at those scales. As an example, Devailly *et al*¹³ quantified long-range viscous interactions between an oscillating probe and a rigid surface fully immersed in a liquid, demonstrating quantitative agreement with lubrication theory. However, these measurements were restricted to rigid interfaces, for which no deformation occurs and the interaction remains purely hydrodynamic. Extending such approaches to deformable interfaces, and in particular to liquid-liquid interfaces, remains a major experimental challenge.

In the present work, we implement this elastohydrodynamic probing scheme using FM-AFM.¹⁴⁻¹⁶ In FM-AFM, a stiff probe oscillates normal to the interface without direct mechanical contact. The resonance frequency shift Δf , and the additional dissipation of the probe, provide simultaneous access to the conservative and dissipative components of the interaction with the interface. The high stiffness and quality factor of the probes ensure sufficient sensitivity in liquid environments while maintaining stable, contactless operation.¹⁷

We first validate this FM-AFM based approach on a reference liquid-solid system, to which the elastohydrodynamic model applies. This validation step establishes the reliability of the measurement protocol and data analysis for separating elastic and viscous contributions. We then apply the same experimental method and analysis to a liquid-liquid system. This configuration constitutes an extreme test case, involving neither solid elasticity nor an established theoretical description. By extending elastohydrodynamic measurements from liquid-viscoelastic systems to liquid-liquid interfaces, this work demonstrates that FM-AFM provides a robust and versatile tool for probing the mechanical response of soft and liquid interfaces under hydrodynamic confinement.

Principle of frequency modulated AFM

In Frequency Modulated Atomic Force Microscopy (FM-AFM) , a probe oscillating at a constant amplitude is locked at its resonance frequency. In the vicinity of an interface, the changes in the resonance frequency and in the energy supplied to the oscillator are respectively related to the elastic and viscous components of the probe/interface interaction.

The oscillator (a quartz tuning fork coupled to a glass fibre in our case) is characterized in air, prior to experiments. Its resonance frequency f_0 serves as the reference, and is expressed as

$$f_0 = \frac{1}{2\pi} \sqrt{\frac{k_{\text{eff}}}{m_{\text{eff}}}},$$

where k_{eff} and m_{eff} are the effective stiffness and mass of the oscillator. A probe/sample interaction results in changes of the effective stiffness Δk and/or mass Δm , and thus shift the resonance frequency to f'_0 . We then measure a frequency shift $\Delta f = f'_0 - f_0$. Considering small variations in stiffness and mass, it is approximated as:

$$\frac{\Delta f}{f_0} \simeq \frac{1}{2} \frac{\Delta k}{k_{\text{eff}}} - \frac{1}{2} \frac{\Delta m}{m_{\text{eff}}}.$$

In fluids, for nanometric oscillation amplitudes, Δm can be safely neglected, the frequency shift predominantly reflecting the conservative interaction through an interaction-induced stiffness k_{int} . It is interpreted as the gradient of the conservative part of the probe/sample interaction force. In these conditions, k_{int} directly relates to the frequency shift :

$$k_{\text{int}} = 2k_{\text{eff}} \frac{\Delta f}{f_0},$$

in small oscillation amplitude approximation.

During experiments, the oscillation amplitude A_0 of the probe is kept constant. Dissipation is then obtained from the variation of the drive amplitude A_D of the oscillator. It can

be expressed as a normalized damping coefficient^{17,18} :

$$\Delta\beta = \beta - \beta_0 = \beta_0 \left(\frac{A_D}{A_{D,0}} - 1 \right),$$

with $\beta_0 = k_{\text{eff}}/(\omega_0 Q)$ the intrinsic damping of the oscillator, and $A_{D,0}$ its drive amplitude in air.

The harmonic response function of the system, or complex mechanical impedance, is defined as the ratio of the amplitude of the interaction force to the amplitude of oscillation at a given oscillation frequency.

$$Z(\omega) = \frac{\tilde{F}_\omega}{\tilde{A}_\omega} = Z'(\omega) + iZ''(\omega),$$

Based on our observables, we can express the moduli of the real and imaginary components of Z at the resonance frequency

$$Z' = 2k_{\text{eff}} \frac{\Delta f}{f_0}, \quad Z'' = \omega \Delta\beta, \quad \omega = 2\pi f_0.$$

This formulation allows direct comparisons with dynamic SFA measurements.¹²

Probe Design and Calibration

Our force probe consists of a cylinder glued to a prong of a quartz tuning fork (QTF), and oscillating along its major axis. The quality factors of these QTF oscillators are much higher than for standard AFM probes, which provides force sensitivities as low as a few tenths of pico newtons per half-hertz. Combined with their high static stiffness, this makes them very suitable for operating close to soft interfaces. Thanks to the hanging fibre design, the oscillator is kept outside the fluid, with only the fibre being dampened. This maintains a high quality factor and therefore high measurement sensitivity.

The cylinders are fabricated from borosilicate glass capillaries tapered using a laser puller

(Sutter Instrument Co., P-2000), yielding capillaries with radii of approximately $2.5 \mu\text{m}$.

A UV-curable adhesive (NOA 81) is used to adhere each fibre perpendicularly to one prong of a QTF (ref. AB26T-32.768KHZ)¹⁸. A $5 \mu\text{m}$ diameter glass microsphere is glued to the fibre apex, as shown in the micrograph of figure 1, in order to define a sphere–plane contact geometry at interfaces, appropriate for quantitative hydrodynamic analysis.

A coupled-oscillator model, which takes into consideration the mechanical coupling between the two prongs, is used to determine the tuning fork’s stiffness from its geometry and the measured frequencies of the symmetric and antisymmetric oscillation modes,¹⁹ without adjustable parameters. A typical value is $k_{\text{eff}} = 4.6 \pm 0.4 \times 10^4 \text{ N/m}$, with a mean quality factor of $Q = 10^4$

We estimate the noise floor²⁰ and determine the electrical sensitivity of our QTFs from measurements of the thermal noise amplitude of the bare oscillator.²¹ Using mean values of the effective stiffness k_{eff} and quality factor Q , we obtain a thermal oscillation amplitude of the tuning fork $A_{\text{th}} = 0.3 \text{ pm}$ at $T = 295.9 \text{ K}$. This corresponds to a force noise density of $1.4 \text{ pN Hz}^{-1/2}$ and to an electrical displacement sensitivity $\alpha = 4.3 \pm 0.4 \text{ nm V}^{-1}$.

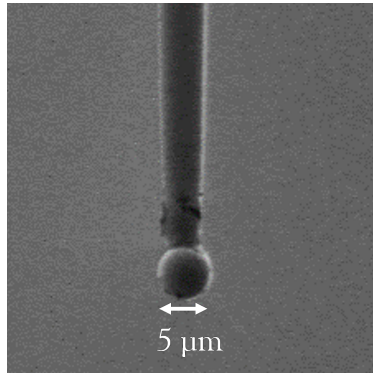


Figure 1: Scanning electron micrograph of the FM-AFM probe. A tapered glass fibre (radius $R = 2.5\mu\text{m}$) is attached perpendicularly to one prong of a quartz tuning fork using a UV-curable adhesive (NOA 81). A glass microsphere of $5\mu\text{m}$ diameter is glued to the fibre apex, defining a well-controlled sphere–plane geometry suitable for elastohydrodynamic measurements. The tuning fork operates at a resonance frequency $f_0 \simeq 32\text{kHz}$, with a quality factor $Q \simeq 10\,000$, a stiffness $k \simeq 46\text{kN.m}^{-1}$, and a typical oscillation amplitude $A_0 = 0.5\text{nm}$.

Table 1: Intrinsic properties of the FM-AFM probe.

Parameter	Symbol / Unit	Value
Resonance frequency	f_0 (kHz)	32
Oscillation amplitude (free)	A_0 (nm)	0.1
Spring constant	k (N/m)	4.6×10^4
Quality factor (air/liquid)	Q	$10^4 / 3-8 \times 10^3$
Tip radius	R (μm)	2.5
Noise floor	δF (pN)	~ 2

Experimental setup

FM-AFM experiments are performed using a vertical custom-built setup optimized for liquid environments previously described.¹⁸ The probe is excited by a piezoelectric actuator, and the vertical motion with respect to the interface is controlled using a linear piezoelectric stage. The entire assembly is enclosed in a sealed chamber with humidity control to minimize evaporation and thermal drift. Before demodulation, the electrical QTF signal is BP filtered and 20dB amplified, using a low-noise SRS-560 differential amplifier. A HF2LI lock-in amplifier demodulates this signal to feed a PLL and a PID feedback loops. PLL loop locks oscillator at resonance frequency by controlling the excitation frequency of the piezo actuator, and monitors the resonance frequency changes (Δf channel). The PID loop keeps oscillation amplitude constant by controlling the drive amplitude of the piezo actuator (dissipation channel). Operating bandwidths of 2 Hz (PLL) and 1 Hz (PID) are used to optimize the signal-to-noise ratios while maintaining stable frequency tracking and amplitude feedback.

Experiments are performed in a rectangular reservoir filled with two immiscible phases arranged in a horizontal layered geometry. In the liquid–liquid configuration, the first liquid is introduced into the reservoir, and the second immiscible liquid is carefully deposited on top to form a flat interface. In the liquid–solid configuration, the bottom phase consists of a cross-linked PDMS layer ($\approx 1\text{mm}$ thickness), covered by a liquid layer.

The FM-AFM probe is positioned above the free surface and vertically displaced across the air–liquid interface, through the upper liquid phase, and toward the liquid–liquid or

liquid–solid interface. The thickness of the upper liquid layer is typically 400–500 μm . This distance was kept as small as practically possible in order to minimize viscous damping of the fibre and preserve a high quality factor, while remaining sufficiently large to avoid perturbations from the air–liquid interface. As both liquids are transparent, and have similar refractive indices, the interface position cannot be determined by a simple optical method during the experiment. As a result, the probe is approached without direct knowledge of its distance to the interface. The position of the interface is subsequently determined from the hydrodynamic signature measured by FM-AFM, as described below.

Approach–retract cycles are performed at a constant speed of 50 nm s^{-1} , much smaller than the characteristic oscillation velocity of the sphere,²² ensuring quasi-static measurement conditions. All measurements are conducted at room temperature in PDMS oils or water–glycerol mixtures of controlled viscosity.

For a typical experiment in a 0.24 Pa s water–glycerol mixture ($\rho \approx 1230 \text{ kg m}^{-3}$, $v = 6 \times 10^{-6} \text{ m s}^{-1}$, $R = 2.5 \text{ }\mu\text{m}$), the Reynolds number is $Re \simeq 2 \times 10^{-7}$, indicating that inertial effects are negligible and that the flow is in the Stokes regime. The hydrodynamic interaction is thus governed by viscous forces, and the confined flow can be described within the lubrication approximation, corresponding to a Poiseuille-type flow in the thin liquid film. This regime is required for the validity of elasto-hydrodynamic models used throughout this work.

Table 2: Experimental parameters used in FM-AFM measurements.

Parameter	Symbol / Unit	Typical Value
Approach velocity	v_a (nm/s)	50
Oscillation velocity	v_o ($\mu\text{m/s}$)	6
Reynolds number	Re	2×10^{-7}
Temperature	T ($^{\circ}\text{C}$)	20–25

Mechanical stability of the fibre probe.

It is necessary to check the mechanical stability of the cantilevered fibre probe before frequency and dissipation shifts can be interpreted. Because of its high aspect ratio, the glass fibre may undergo lateral deflections under axial loading. The probe would experience lateral deflections as a result of this coupling, leading to frequency and dissipation shifts unrelated to the intrinsic interfacial mechanical response.

The onset of buckling is estimated using Euler's column theory.²³ Since the probe consists of a hollow cylindrical glass capillary, its bending stiffness is characterized by the second moment of area

$$I = \frac{\pi}{64} (d_o^4 - d_i^4),$$

where $d_o = 5 \mu\text{m}$ is the outer diameter and $d_i \simeq 1.8 \mu\text{m}$ the inner diameter of the fibre. The corresponding critical buckling load is

$$P_{\text{cr}} = \frac{\pi^2 E_f I}{(KL)^2},$$

with $E_f \approx 70 \text{ GPa}$ is the Young's modulus of borosilicate glass, $L = 3 \text{ mm}$ the effective length of the fibre, and $K = 2$ the boundary condition factor for a fixed-free geometry. This yields a critical buckling force $P_{\text{cr}} \simeq 5.8 \times 10^{-7} \text{ N}$. To relate this axial load to the experimental indentation depth, we use Hertzian contact mechanics²⁴ for a sphere of radius $R = 2.5 \mu\text{m}$ indenting an elastic substrate:

$$P = \frac{4}{3} E^* \sqrt{R} \delta^{3/2}, \quad E^* = \frac{E_s}{1 - \nu^2},$$

where E_s is the Young's modulus of the substrate and ν its Poisson ratio ($\nu = 0.48$ for PDMS). Solving for δ at $P = P_{\text{cr}}$ gives the critical indentation depth

$$\delta_{\text{cr}} = \left(\frac{3P_{\text{cr}}}{4E^*\sqrt{R}} \right)^{2/3}.$$

For the stiffest PDMS investigated ($E_s = 2.7$ MPa), this yields $\delta_{cr} \simeq 180$ nm.

Since FM-AFM directly measures the interaction stiffness $Z' = dP/d\delta$, it is useful to express this limit in terms of a critical stiffness. Differentiating the Hertz relation gives

$$Z = \frac{dP}{d\delta} = 2E^* \sqrt{R\delta}.$$

Evaluating at $\delta = \delta_{cr}$ yields the critical interaction stiffness

$$Z_{cr} = 2E^* \sqrt{R\delta_{cr}} = \frac{3}{2} \frac{P_{cr}}{\delta_{cr}} \approx 4.8 \text{ N.m}^{-1}$$

This value defines the maximum interaction stiffness that can be applied while maintaining axial stability of the fibre probe. For $Z < Z_{cr}$, the probe remains mechanically stable and the measured impedance reflects the interfacial response. For Z approaching Z_{cr} , probe compliance and the onset of buckling may affect the measurements, and data points approaching this threshold were excluded from quantitative analysis. Using this Euler–Hertz estimate, the corresponding critical indentation depth for stable operation lies in the range $\delta_{cr} \approx 180$ – 200 nm. For the stiffest PDMS substrate ($E_s = 2.7$ MPa), the measured interaction stiffness approached this threshold, indicating that probe mechanics rather than interfacial mechanics limited the accessible range. In contrast, for softer substrates ($E_s = 0.4$ – 1.2 MPa), the interaction stiffness remained well below Z_{cr} , and probe stability is not a limiting factor. This constraint does not apply to liquid–liquid interfaces, where the absence of bulk elasticity prevents significant axial compression of the probe.

Results and discussion

FM-AFM Observables

During approach-retract cycles, the normalized frequency shift $\Delta f/f_0$ and the excess dissipation are recorded as a function of the probe vertical position. These signals provide access,

in the vicinity of the interface, to the conservative and dissipative components of the sphere interface interaction mediated by the confined liquid film.

In the bulk hydrodynamic regime, where the interface does not affect the probe motion, both signals vary linearly with the immersion depth due to viscous drag. This regime corresponds to hydrodynamic loading by the bulk liquid, whose magnitude depends on the liquid viscosity, density and varies linearly with the penetration depth.¹⁸ Other studies have focused on the rheology of simple fluids,^{25,26} but here we focus on the intrinsic behaviour of the interface. Thus, to isolate the interfacial contributions, the hydrodynamic linear background is subtracted from both signals. The corrected data are then converted into the real and imaginary components of the complex mechanical impedance, $Z = Z' + iZ''$. The real component Z' reflects the elastic response of the interface, while the imaginary component Z'' corresponds to viscous dissipation within the liquid film confined between the probe and the interface. These components are used throughout this work to characterize interfacial properties under hydrodynamic confinement.

Reference Liquid-Solid Interface

We first apply the FM-AFM hydrodynamic probing scheme to a reference liquid-solid system consisting in a water-glycerol mixture confined against a cross-linked PDMS thick film ($E = 2.7\text{MPa}$). In this configuration, the elastohydrodynamic (EHD) framework provides a quantitative description of the oscillatory drainage of a thin liquid film of thickness D confined between the rigid sphere and an elastic interface. In this regime, the hydrodynamic pressure remains approximately constant within a zone of radial extension $\sim \sqrt{RD}$, resulting in a uniform elastic deformation of the substrate.

Figure 2 shows the raw signals recorded during the approach. Both the normalized resonance frequency shift $\Delta f/f_0$ and the dissipation signal vary linearly with immersion depth in the bulk liquid, reflecting viscous drag. After subtraction of this contribution, the real and imaginary parts of the mechanical impedance, Z' and Z'' , are calculated.

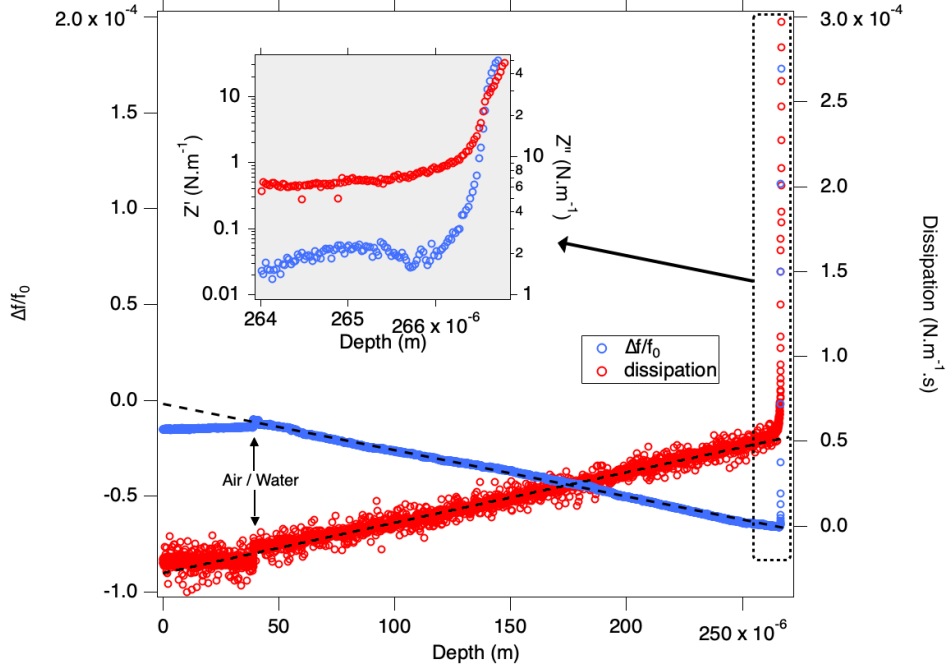


Figure 2: Raw AFM signals recorded during the approach of the oscillating probe toward a cross-linked PDMS thick film ($E = 2.7\text{MPa}$) in a water-glycerol mixture. The normalized resonance frequency shift $\Delta f/f_0$ (blue triangles, left axis) and the dissipation signal (red circles, right axis) are plotted as a function of probe depth. After entering the liquid (vertical arrows), both observables exhibit a linear dependence on depth (dashed lines), characteristic of viscous drag in the bulk liquid, followed by a transition towards interfacial confinement and deformation. After subtraction of the bulk liquid contribution, the inset shows the real (Z' , blue) and imaginary (Z'' , red) components of the mechanical impedance as a function of depth.

In the hydrodynamic regime, where no elastic deformation occurs, the interaction is governed by Reynolds lubrication theory. In the sphere–plane geometry, it gives an expression for the dissipative impedance:^{9,27}

$$Z''(\omega) = \frac{6\pi\eta R^2\omega}{D},$$

where D is the distance to the undeformed interface. Consequently, $1/Z''$, the mobility, varies linearly with D and can be used to determine the absolute interface position by extrapolation to zero mobility, known as the hydrodynamic zero.²⁸

Figure 3 shows such an analysis of the evolution of Z'' on cross-linked PDMS, which

allows us to determine the initial position of the interface.

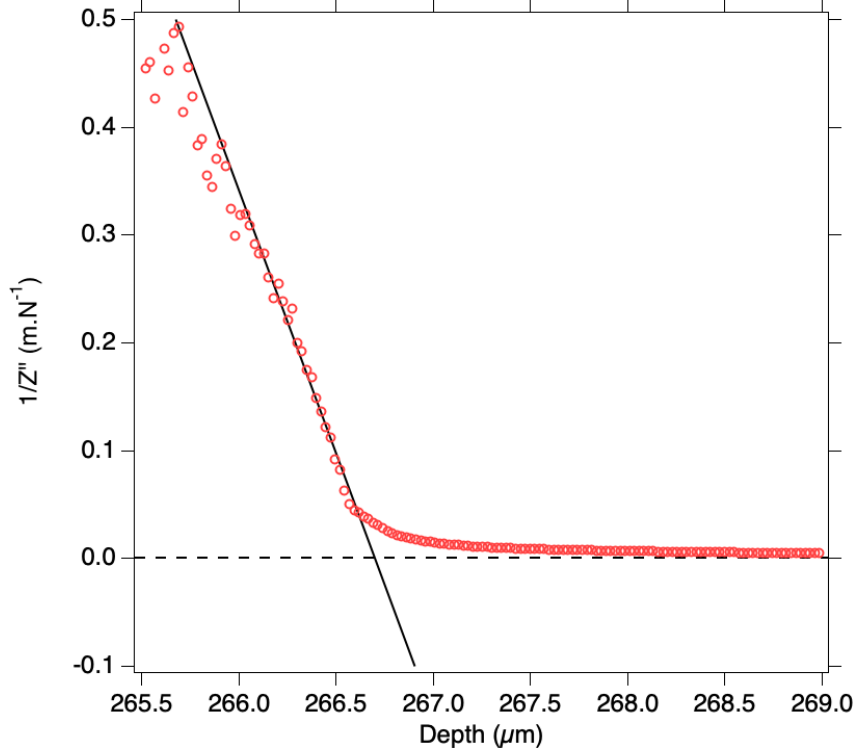


Figure 3: Determination of the confined liquid film thickness d_c at the water-glycerol / cross-linked PDMS interface ($E = 2.7\text{MPa}$, $\eta = 0.013\text{Pa.s}$, $T = 22\text{ }^\circ\text{C}$). The inverse dissipative component of the mechanical impedance, $1/Z''$, the mobility, is plotted as a function of the probe-interface separation. At large separations, $1/Z''$ follows a linear hydrodynamic regime characteristic of viscous drainage. At smaller separations, the signal reaches a plateau corresponding to the confinement regime. The extrapolation to zero of the linear hydrodynamic regime defines the position of the undeformed interface. We deduce a value of $D_c = 135 \pm 20\text{nm}$ from the distance at which $1/Z''$ deviates from a purely viscous response with respect to the position of the undeformed interface.

We also determine the confinement thickness from the distance with respect to the position of the undeformed interface, at which $1/Z''$ deviates from a purely viscous response. This analysis yields $D_c = 135 \pm 20\text{ nm}$, in quantitative agreement with the elasto-hydrodynamic prediction,

$$D_c = 8R \left(\frac{\eta\omega}{E^*} \right)^{2/3},$$

which gives $D_c = 154\text{ nm}$ for the present experimental parameters.

Using this reference position, the impedance components can be plotted as a function of the distance to the undeformed interface (Fig. 4). In this representation, we clearly distinct two regimes. Far from the interface, the dissipative component follows the Reynolds scaling $Z'' \propto D^{-1}$, with a measured exponent of -0.94 ± 0.03 . Simultaneously, the elastic component follows the elastohydrodynamic prediction $Z' \propto D^{-5/2}$, with a measured exponent of -2.6 ± 0.1 , in quantitative agreement with the theoretical value. At approximately 300nm from the interface (indicated by arrows in the figure 4), the impedance exceeds the critical value defined above, and fibre buckling occurs. However, this did not prevent us from determining the elastohydrodynamic scaling and does not affect the quantitative agreement with the model.

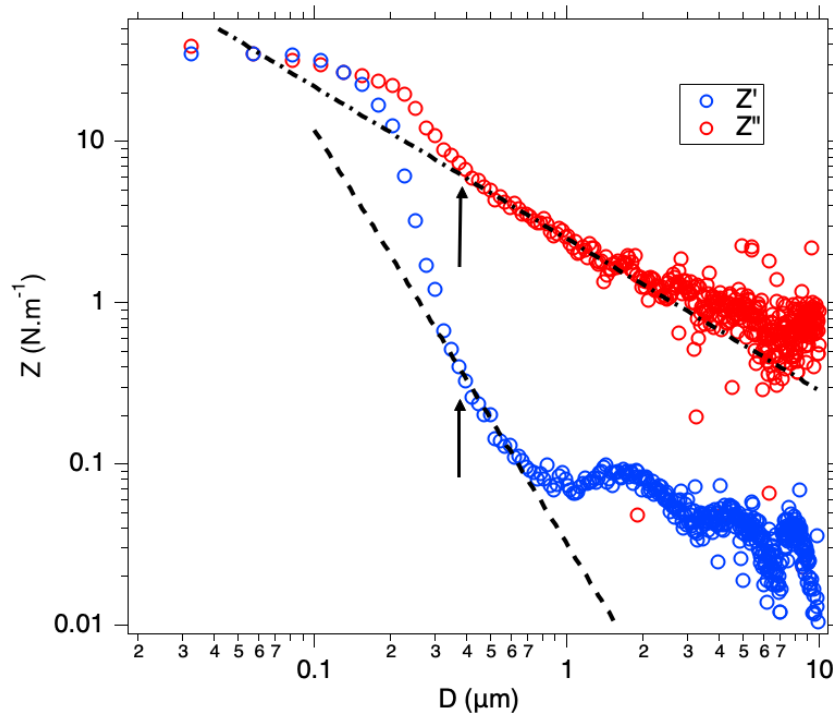


Figure 4: Plot of the real and imaginary parts of the mechanical impedance, at the water-glycerol cross-linked PDMS interface ($E = 2.7\text{MPa}$, $\eta = 0.013\text{Pa.s}$, $T = 22^\circ\text{C}$), as a function of the probe- undeformed interface distance. Showing, as the probe moves closer to the interface, the transition from viscous behaviour to elastic deformation, where both components saturate at similar values, as expected for a bulk viscoelastic material. In the elastic deformation regime before saturation, Z'' follows a $D^{-0.94 \pm 0.03}$ power law, while Z' follows a $D^{-2.6 \pm 0.1}$ law. The arrows indicate the distance beyond which fibre buckling occurs (see text for details).

As the probe approaches closer than D_c , viscous drainage is inhibited and the hydrodynamic pressure is transmitted to the elastic substrate, which deforms in response to the oscillatory loading. In this regime, both impedance components saturate to comparable values.

To further validate this elastohydrodynamic description, we then vary the Young’s modulus of the cross-linked PDMS and reproduced the experiment. The resulting measured confinement thicknesses $D_c(E)$ are plotted in Fig.5.

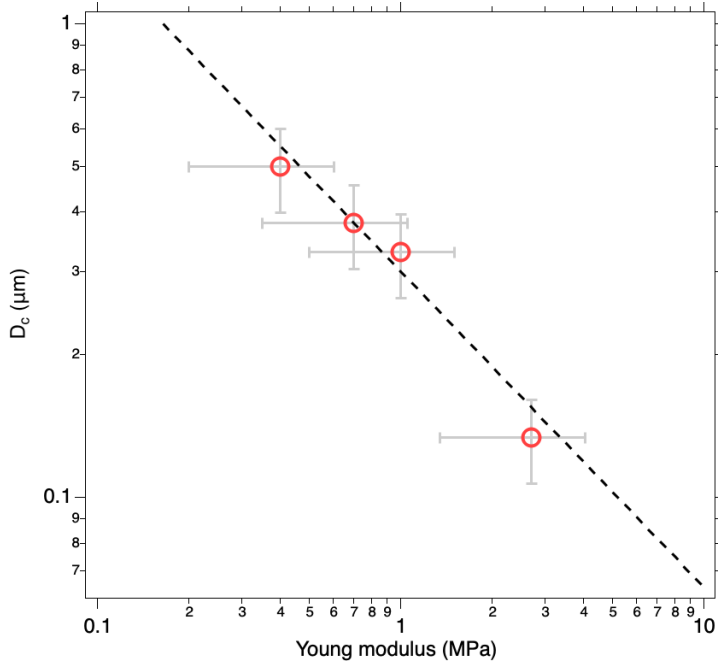


Figure 5: Confinement thickness D_c measured at the water–glycerol / cross-linked PDMS interface as a function of the Young’s modulus E of the elastomer (symbols). The dashed line shows the elastohydrodynamic prediction $D_c = 8R(\eta\omega/E^*)^{2/3}$. Experimental uncertainty on D_c arises from the resolution of the positioning stage and from the determination of the hydrodynamic zero. The agreement with the theoretical trend confirms the quantitative reliability of the method.

The measured confinement thickness follows the predicted scaling $D_c \propto E^{-2/3}$, in quantitative agreement with elastohydrodynamic model. This liquid–solid reference system therefore provides a quantitative validation of the FM-AFM hydrodynamic probing method.

Liquid-Liquid Interface

The FM-AFM measurements are then performed on a liquid-liquid interface composed of two immiscible viscous phases: a PDMS oil phase ($\eta_{PDMS} = 0.019\text{Pa}\cdot\text{s}$) and a water-glycerol mixture ($\eta_{aq} = 0.246\text{Pa}\cdot\text{s}$). We use a highly viscous aqueous phase to slow down drainage and increase the mechanical resistance of the interface, thereby approaching conditions comparable to a liquid-solid interface. Increasing the viscosity of the lower phase enhances the hydrodynamic stresses transmitted to the interface and eases quantitative measurements of interfacial mechanical response.

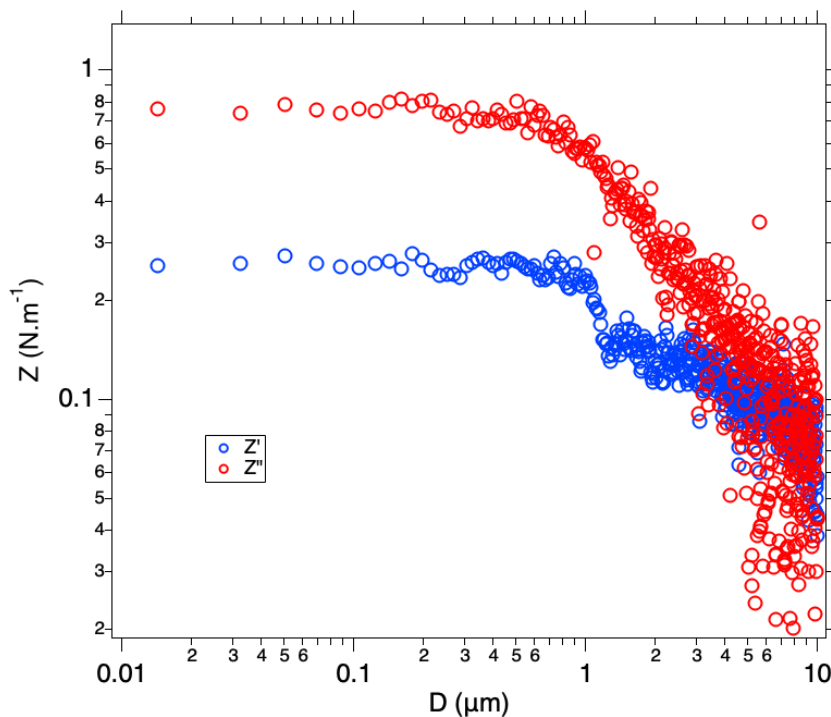


Figure 6: Real (Z') and imaginary (Z'') components of the mechanical impedance measured by FM-AFM during the approach toward a fully liquid-liquid interface composed of PDMS ($\eta_{PDMS} = 0.019\text{Pa}\cdot\text{s}$) and a water-glycerol mixture ($\eta_{aq} = 0.246\text{Pa}\cdot\text{s}$), at $T = 22\text{ }^\circ\text{C}$. The probe approached quasi-statically at $v_{app} = 50\text{nm}\cdot\text{s}^{-1}$ with an oscillation velocity $v_{osc} = 6\mu\text{m}\cdot\text{s}^{-1}$. The impedance components are plotted as a function of the probe-interface separation for a glass microsphere of radius $R = 2.5\mu\text{m}$. Both Z' and Z'' remain significantly smaller than for a liquid-solid interface, reflecting the absence of bulk solid elasticity and a predominantly viscous response governed by hydrodynamic drainage and interfacial deformation.

Figure 6 shows the real and imaginary components of the mechanical impedance mea-

sured during the approach toward the liquid–liquid interface. As in the liquid–solid configuration, a transition is observed between a distance-dependent hydrodynamic regime at large separations and a plateau at short distances. This plateau defines the confinement thickness, corresponding to the transition between purely hydrodynamic drainage and interfacial deformation.

Compared to the liquid–solid reference system, both impedance components are reduced by more than one order of magnitude, and impedance components saturate to different values. Notably, Z' and Z'' exhibit an equivalent D^{-1} dependence, characteristic of a predominantly viscous response. The saturation value of the elastic impedance is measured as $Z'_{\text{sat}} = 108 \pm 20 \text{ mN m}^{-1}$, while the equilibrium interfacial tension of the same system is $\gamma = 37 \pm 1 \text{ mN m}^{-1}$.

The confinement thickness is extracted from the inverse dissipative impedance, $1/Z''$, following the same procedure as for the liquid–solid interface. A value of $D_c = 1.07 \pm 0.1 \mu\text{m}$ is obtained, approximately one order of magnitude larger than the one measured for the liquid–solid interface. This confirms the much higher deformability of liquid–liquid interfaces compared to elastic solids.

Discussion

The most stringent test of the FM-AFM hydrodynamic probing method is provided by the liquid–liquid interface, where both contacting phases are deformable and no bulk elasticity contributes to the mechanical response. In contrast with liquid–solid systems, where the no-slip boundary condition imposes zero velocity at the interface and leads to classical Poiseuille drainage, a liquid–liquid interface allows interfacial motion. As a result, the flow field and stress distribution differ fundamentally from the elastohydrodynamic framework. Figure 7, which shows the plot of the inverse impedance as a function of distance from the interface of the two systems studied, illustrates this difference.

As noted above, for the liquid interface both impedance components are reduced by more

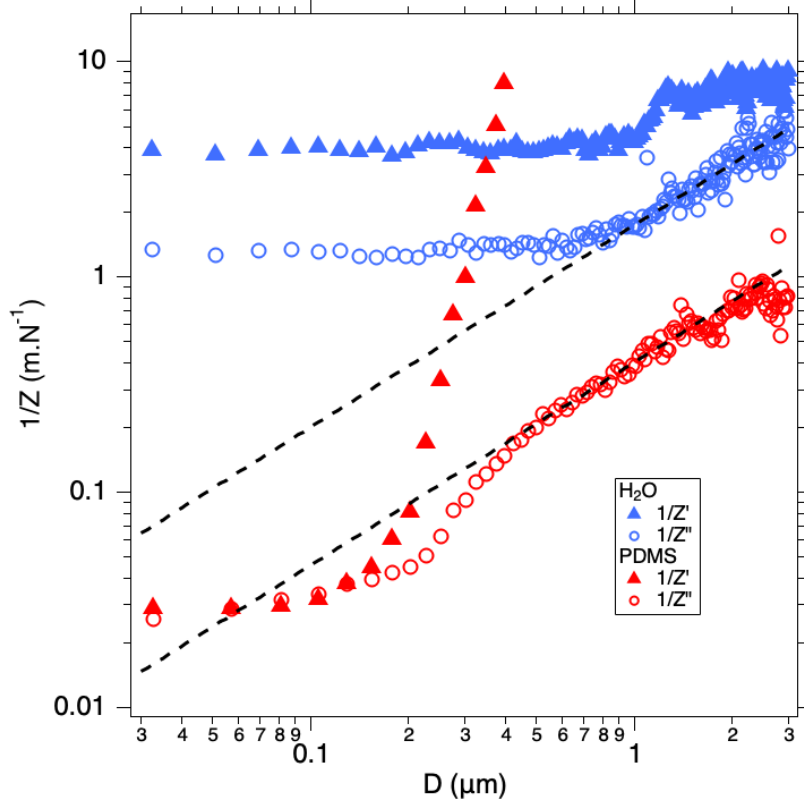


Figure 7: Real (solid triangle) and imaginary (hollow circles) components of the inverse of mechanical impedance as a function of distance from the interface, . For the water cross-linked PDMS system (in red) and PDMS oil water system (in blue). The two imaginary components, corresponding to viscous drainage, vary linearly with D (dotted lines for guidance). While the real part for the liquid interface also shows a viscous response of limited amplitude, the cross-linked PDMS interface shows a response typical of a viscoelastic material, with an amplitude that is an order of magnitude greater than that of the liquid interface. Deformation of the liquid interface occurs at a critical distance $D_c = 1.07 \pm 0.1 \mu\text{m}$, whereas $D_c = 135 \pm 20 \text{nm}$ for the cross-linked PDMS interface.

than one order of magnitude compared to the liquid–solid reference system, and exhibit a D^{-1} dependence. The elastic impedance saturates at $Z'_{\text{sat}} = 108 \pm 20 \text{ mN m}^{-1}$, while the interfacial tension is only $\gamma = 37 \pm 1 \text{ mN m}^{-1}$. This difference demonstrates that the in-phase mechanical response cannot be attributed solely to static capillary forces.

The fact that Z' varies in D^{-1} , and that the saturation value associated to the deformation significantly differs from the interfacial tension of the PDMS–water system, suggests a viscous response from the interface reminiscent of a complex liquid.

Quantitatively, the confinement thickness increases from $D_c \approx 0.1 \mu\text{m}$ in the liquid–solid

case to $D_c \approx 1.1\mu\text{m}$ in the liquid–liquid configuration. This order-of-magnitude increase directly reflects the absence of bulk elastic restoring forces and the enhanced deformability of the interface.

The EHD model cannot be directly applied to this configuration. It assumes that the interfacial velocity is zero in the absence of slip. While this condition is satisfied for a liquid/solid interface, for a liquid/liquid interface the interfacial velocity may be non-zero. These conditions differ from Poiseuille flow.

In the liquid–solid configuration, the hydrodynamic pressure generated within the confined liquid film is transmitted uniformly to the elastic substrate, producing a well-defined elastic restoring force. In contrast, for a liquid–liquid interface, this pressure induces interfacial motion and viscous flow rather than elastic compression, so that the mechanical response is governed by viscous stresses and interfacial hydrodynamics.

These results demonstrate that, even in the absence of bulk elasticity, the weak mechanical response of liquid interfaces can be measured by this technique. We show that this response under hydrodynamic confinement is governed by viscous stresses at the interface rather than elastic restoring forces. Such a behaviour is characteristic of complex fluid interfaces, including polymer films, biological membranes, and capsules, where interfacial viscosity and flow determine the mechanical response.

Conclusion

We have developed a frequency-modulation AFM method to probe liquid interfaces under hydrodynamic confinement in a strictly contactless manner. Using a hanging fibre probe, both the dissipative and elastic components of the mechanical impedance, as well as the confinement thickness, can be measured quantitatively with nanometric resolution.

The method was first validated on a reference liquid–solid interface, where quantitative agreement with the elastohydrodynamic model confirmed its ability to resolve the coupled

viscous and elastic dynamics of confined liquid films. It was then successfully applied to a liquid–liquid interface, where no bulk elasticity is present.

The original measurements presented here show an essentially viscous response for a liquid interface, and suggest that the in-phase component of the measured mechanical impedance could be related to a non-zero flow velocity at the interface.

This demonstrates that hydrodynamic confinement can be used as a sensitive, quantitative, and fully contactless probe of interfacial mechanics, even in systems where no solid reference exists. More broadly, this approach provides a new experimental framework for investigating the micromechanics of soft and complex interfaces. In particular, it opens promising perspectives for studying viscoelastic and non-Newtonian interfaces such as biological membranes, polymer films, vesicles, and membranes where interfacial flow and confinement play a central role in determining mechanical response.

The use of this technique, in which a fluid flow becomes the probe, also allows the applied stress to be finely adjusted by controlling the viscosity of the fluid phase. This can be a major advantage for studying highly deformable systems.

This establishes FM-AFM as a promising tool for quantitative interfacial micro-rheology.

References

- (1) De Gennes, P.-G.; Brochard-Wyart, F.; Quéré, D. *Capillarity and Wetting Phenomena*; Springer New York: New York, NY, 2004.
- (2) De Gennes, P. G. Wetting: statics and dynamics. *Rev. Mod. Phys.* **1985**, *57*, 827–863.
- (3) Langmuir, I. The constitution and fundamental properties of solids and liquids. *J. Am. Chem. Soc.* **1917**, *39*, 1848–1906.
- (4) Wilhelmy, L. Ueber die Bestimmung der Oberflächenspannung von Flüssigkeiten. *Annalen der Physik* **1863**, *119*, 177–191.

- (5) Hartland, S.; Ramakrishnan, S.; Hartley, R. The Oscillation of Drops and Spheres at Fluid—Liquid Interfaces. *Chem. Eng. Sci.* **1975**, *30*, 1141–1148.
- (6) Freer, E. M.; Wong, H.; Radke, C. J. Oscillating Drop/Bubble Tensiometry: Effect of Viscous Forces on the Measurement of Interfacial Tension. *J. Coll. Int. Sci.* **2005**, *282*, 128–132.
- (7) Hochmuth, R. M. Micropipette Aspiration of Living Cells. *J. Biomechanics* **2000**, *33*, 15–22.
- (8) Tadros, T. Viscoelastic properties of sterically stabilised emulsions and their stability. *Adv. Coll. Int. Sci.* **2015**, *222*, 692–708.
- (9) Vinogradova, O. I. Drainage of a thin liquid film confined between hydrophobic surfaces. *Langmuir* **1995**, *11*, 2213–2220.
- (10) Vinogradova, O. I. Slippage of water over hydrophobic surfaces. *Int. J. Min. Proc.* **1999**, *56*, 31–60.
- (11) Liron, N.; Shahar, R. Stokes flow due to a Stokeslet in a pipe. *J. Fluid Mech.* **1976**, *86*, 727–744.
- (12) Leroy, S.; Charlaix, E. Hydrodynamic interactions for the measurement of thin film elastic properties. *J. Fluid Mech.* **2011**, *674*, 389–407.
- (13) Devailly, C.; Bouriat, P.; Dicharry, C.; Risso, F.; Ondarçuhu, T.; Tordjeman, P. Long-range hydrodynamic forces in liquid FM-AFM. *Nanotechnology* **2020**, *31*, 455501.
- (14) Giessibl, F. Advances in atomic force microscopy. *Rev. Mod. Phys.* **2003**, *75*, 949–983.
- (15) Albrecht, T. R.; Grütter, P.; Horne, D.; Rugar, D. Frequency Modulation Detection Using High-Q Cantilevers for Enhanced Force Microscope Sensitivity. *J. Appl. Phys.* **1991**, *69*, 668–673.

- (16) Garcia, R.; Perez, R. Dynamic Atomic Force Microscopy Methods. *Surf. Sci. Rep.* **2002**, *47*, 197–301.
- (17) Ondarçuhu, T.; Aimé, J.-P. *Nanoscale liquid interfaces: Wetting, patterning and force microscopy at the molecular scale*; CRC Press, 2013.
- (18) Rocheron, M.; Curtil, C.; Klein, H. R. FM-AFM with a Hanging Fiber Probe for the Study of Liquid–Liquid Interfaces. *Langmuir* **2022**, *38*, 6592–6601.
- (19) Castellanos-Gomez, A.; Agraït, N.; Rubio-Bollinger, G. Dynamics of quartz tuning fork force sensors used in scanning probe microscopy. *Nanotechnology* **2009**, *20*, 215502.
- (20) Butt, H.-J.; Jaschke, M. Calculation of thermal noise in atomic force microscopy. *Nanotechnology* **1995**, *6*, 1–7.
- (21) Welker, F., J de Faria Elsner; Giessibl, F. Application of the equipartition theorem to the thermal excitation of quartz tuning forks. *Appl. Phys. Lett.* **2011**, *99*, 084102.
- (22) $v_{max} \approx 6 \mu\text{m s}^{-1}$ for an oscillation amplitude of 0.5 nm at $f_0 = 32$ kHz.
- (23) Timoshenko, S. *Theory of Elastic Stability*; McGraw-Hill Book Company: New York and London, 1936.
- (24) Johnson, K. L. *Contact mechanics*; Cambridge university press, 1985.
- (25) Sandoval, F.; Sepulveda, M.; Bellon, L.; Melo, F. High resolution viscosity measurements by thermal noise detection. *Sensors* **2015**, *15*, 27905–27916.
- (26) Xiong, X.; Guo, S.; Xu, Z.; Sheng, P.; Tong, P. Development of an atomic-force-microscope based hanging fiber rheometer for interfacial microrheology. *Phys. Rev. E* **2009**, *80*, 061604.
- (27) Israelachvili, J. *Intermolecular and Surface Forces, 3rd Edition*; 2011.

- (28) Canale, L.; Comtet, J.; Niguès, A.; Cohen, C.; Clanet, C.; Siria, A.; Bocquet, L.
Nanorheology of Interfacial Water during Ice Gliding. *Phys. Rev. X* **2019**, *9*, 041025.